THE JOURNAL OF BIOLOGICAL CHEMISTRY VOL. 291, NO. 17, pp. 9244–9256, April 22, 2016

Conformational Dynamics and Allostery in Pyruvate Kinase*

Received for publication, July 2, 2015, and in revised form, February 4, 2016 Published, JBC Papers in Press, February 15, 2016, DOI 10.1074/jbc.M115.676270

Katherine A. Donovan[‡1], Shaolong Zhu[§], Peter Liuni[§], Fen Peng[¶], Sarah A. Kessans[‡], Derek J. Wilson[§‖2], and Renwick C. J. Dobson[‡3]**

*From the [‡]Biomolecular Interaction Centre and School of Biological Sciences, University of Canterbury, Private Bag 4800, Christchurch 8041, New Zealand, [§]Department of Chemistry, York University, Toronto, Ontario M3J 1P3, Canada, [¶]Biology and Biochemistry, University of Houston, Houston, Texas 77204, [‖]Centre for Research in Mass Spectrometry, Department of Chemistry, York University, 4700 Keele Street, Toronto, Ontario M3J 1P3, Canada, and **Department of Biochemistry and Molecular Biology, Bio21 Molecular Science and Biotechnology Institute, University of Melbourne, 30 Flemington Road, Parkville, Victoria 3010, Australia*

Pyruvate kinase catalyzes the final step in glycolysis and is allosterically regulated to control flux through the pathway. Two models are proposed to explain how *Escherichia coli* pyruvate kinase type 1 is allosterically regulated: the "domain rotation model" suggests that both the domains within the monomer and the monomers within the tetramer reorient with respect to one another; the "rigid body reorientation model" proposes only a reorientation of the monomers within the tetramer causing rigidification of the active site. To test these hypotheses and elucidate the conformational and dynamic changes that drive allostery, we performed time-resolved electrospray ionization mass spectrometry coupled to hydrogen-deuterium exchange studies followed by mutagenic analysis to test the activation mechanism. Global exchange experiments, supported by thermostability studies, demonstrate that fructose 1,6-bisphosphate binding to the allosteric domain causes a shift toward a globally more dynamic ensemble of conformations. Mapping deuterium exchange to peptides within the enzyme highlight site-specific regions with altered conformational dynamics, many of which increase in conformational flexibility. Based upon these and mutagenic studies, we propose an allosteric mechanism whereby the binding of fructose 1,6-bisphosphate destabilizes an α-helix that bridges the allosteric and active site domains within the monomeric unit. This destabilizes the β-strands within the $(\beta/\alpha)_8$-barrel domain and the linked active site loops that are responsible for substrate binding. Our data are consistent with the domain rotation model but inconsistent with the rigid body reorientation model given the increased flexibility at the interdomain interface, and we can for the first time explain how fructose 1,6-bisphosphate affects the active site.

Allostery is the effect that ligand binding at one site on a macromolecule has on the physicochemical properties of another, topographically distinct site (1–5). Allostery provides immediate enzymatic control of reaction flux in response to cellular signals (*e.g.* the feedback regulation of a branch point enzyme by the concentration of the pathway product). As such, allostery is critical for the modulation of cellular metabolism and is ubiquitous across all forms of life.

Pyruvate kinase (EC 2.7.1.40) catalyzes the final step in the central energy production pathway, glycolysis (6, 7), and as such is a key enzyme in cellular metabolism. It mediates a phosphate transfer from phosphoenolpyruvate to ADP, producing pyruvate and ATP (Fig. 1*A*). Pyruvate, and to a lesser extent phosphoenolpyruvate, are common precursors in metabolism, including the synthesis of glucose, fatty acids, glycerol, and amino acids (8). Thus, it is essential that pyruvate and phosphoenolpyruvate are maintained at appropriate concentrations in response to the needs of the cell (9).

Not surprisingly, pyruvate kinase enzymes are almost always allosterically regulated. Moreover, cells often express multiple pyruvate kinase isozymes that are regulated by different effectors. The isozymes are usually homotropically activated by the substrate phosphoenolpyruvate to allow regulation of the glycolytic flux in response to elevated phosphoenolpyruvate levels (10). In addition, they are often heterotropically regulated by various allosteric effectors whose chemical nature depends on the organism or tissue (8, 11). For example, *Escherichia coli* has two pyruvate kinase enzymes that are regulated by different allosteric activators. The type 1 pyruvate kinase, the focus of this work, is heterotropically activated by fructose 1,6-bisphosphate. The binding of fructose 1,6-bisphosphate has a K-type effect whereby it increases the affinity of the enzyme for the substrate, phosphoenolpyruvate (12). In contrast, pyruvate kinase type 2 is heterotropically activated by AMP (13, 14).

Key to unraveling allosteric mechanisms are the structures of the enzyme with and without bound allosteric effectors. Atomic resolution x-ray structures of pyruvate kinase enzymes from mammalian, bacterial, and parasitic organisms have been reported (7, 8, 10, 11, 15–18). As is common in allosterically controlled enzymes, pyruvate kinase is oligomeric and is usually a homotetramer. Each monomer comprises three or four domains: A, B, C, and N-terminal domains (only present in mammalian enzymes) (11) (Fig. 1, *B* and *C*). The A-domain is a $(\beta/\alpha)_8$-barrel (TIM barrel) housing the active site at the top of

* The authors declare that they have no conflicts of interest with the contents of this article.

[1] Supported by Maurice Wilkins Centre flexible research funding and a Journal of Cell Science travel fellowship.

[2] Supported by a Natural Sciences and Engineering Research Council of Canada discovery grant. To whom correspondence may be addressed. Tel.: 416-736-2100 (ext. 20786); Fax: 416-736-5936; E-mail: dkwilson@yorku.ca.

[3] Supported in part by Ministry of Business, Innovation and Employment Contract UOCX1208, New Zealand Royal Society Marsden Fund Contract UOC1013, and United States Army Research Laboratory and United States Army Research Office Contract/Grant W911NF-11-1-0481. To whom correspondence may be addressed: Biomolecular Interaction Centre, School of Biological Sciences, University of Canterbury, Private Bag 4800, Christchurch, New Zealand. Tel.: 64-3-364-2987; Fax: 64-3-364-2590; E-mail: renwick.dobson@canterbury.ac.nz.

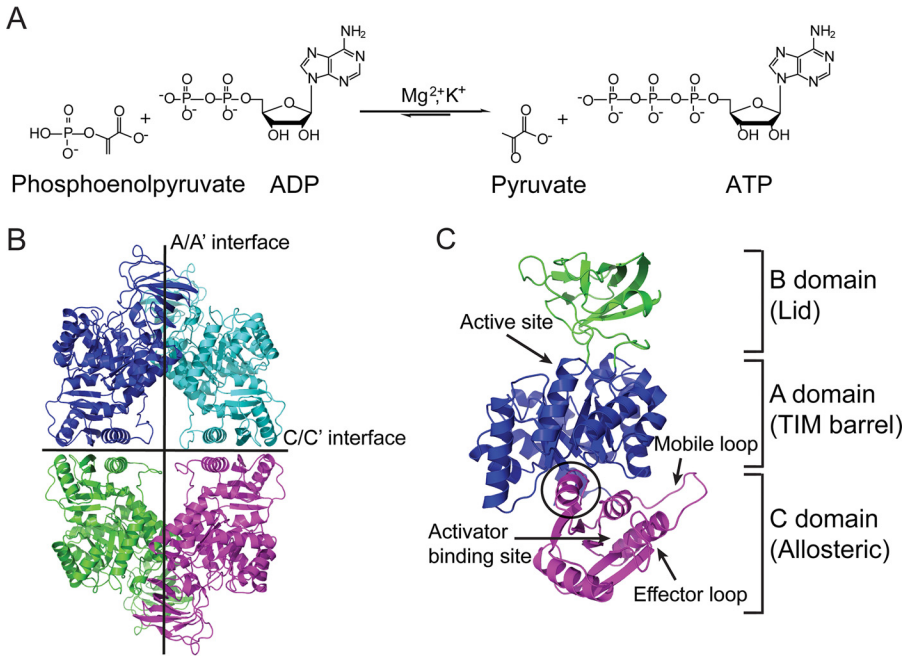

FIGURE 1. *A*, the reaction catalyzed by pyruvate kinase. *B*, structure of *E. coli* pyruvate kinase type 1 tetramer with the tetrameric A/A′ and C/C′ interfaces labeled. *C*, pyruvate kinase type 1 monomer showing the active site and allosteric binding site. The monomer is colored by domain, and the helix that connects the allosteric domain with the active site domain is *circled*.

the barrel. The B-domain, also known as the "lid domain," is thought to close over the active site upon substrate binding. The active site is located in the cleft between the A- and B-domains, and this is where the essential mono- and divalent cations bind (19). The C-domain consists of five α-helices and five strands of mixed β-sheets housing the allosteric binding site close to the tetrameric interface (8, 17). Finally, the N-terminal domain is a short α-helical extension preceding the $(\beta/\alpha)_8$-barrel domain whose role is less defined (11).

To unpick the molecular mechanism(s) by which pyruvate kinase achieves allosteric control upon fructose 1,6-bisphosphate binding, several groups have determined the three-dimensional crystal structures of various isozymes in both the allosteric activator-bound and -unbound states (10, 11, 17, 18).

The fructose 1,6-bisphosphate-bound structures reveal that the allosteric activator binding site is located entirely within the C-domain and must transmit an allosteric signal over a 40-Å distance to the active site in the same subunit. The binding site is located in a pocket formed from an effector loop and the first two turns of the Cα5′-helix in *Saccharomyces cerevisiae* (11) and human liver (20) pyruvate kinases. Fructose 1,6-diphosphate binds in the equivalent pocket in *Leishmania mexicana* (17), *Trypanosoma cruzi* (10), and *Trypanosoma brucei* (21). Structural studies in *L. mexicana* (17) and *T. cruzi* (10) suggest that the allosteric transition involves a rigid body rocking motion of the A- and C-domains that reorients these domains within the tetramer.

Based largely on structural studies, two models have been proposed by others to explain how *E. coli* pyruvate kinase type 1 is regulated by fructose 1,6-bisphosphate (Fig. 2) The first suggests that the domains within the monomer are reoriented along with changes in the orientation of the monomers within the tetramer (8, 22, 23) (Fig. 2*A*). The second competing model puts forward that the domains are rigid and that reorientation of the domains within the tetramer causes the active site to rigidify, presumably in a conformation that better binds the substrate phosphoenolpyruvate (10, 17) (Fig. 2*B*).

The structure of *E. coli* pyruvate kinase type 1 isozyme with fructose 1,6-bisphosphate bound is lacking. Previous attempts by us and others (8) to soak fructose 1,6-bisphosphate into *E. coli* pyruvate kinase type 1 crystals have caused them to crack. This indicates that fructose 1,6-bisphosphate binding causes conformational changes that affect crystal packing. Moreover, our attempts to co-crystallize *E. coli* pyruvate kinase type 1 with fructose 1,6-bisphosphate have not yielded crystals, despite using large and sparse matrix screens that can trial >1000 different conditions and successfully obtaining unliganded enzyme crystals in various conditions. One explanation for this is that the fructose 1,6-bisphosphate-bound protein is heterogeneous in some way.

To build a detailed picture of the conformational and dynamic changes that drive *E. coli* pyruvate kinase type 1 heterotopic allosteric activation by fructose 1,6-bisphosphate, we performed time-resolved electrospray ionization mass spectrometry coupled to a hydrogen-deuterium exchange study. The "new view" of allostery describes a dynamic process whereby a protein fluctuates within an ensemble of conformations (24–27). Although the concept of allostery has evolved considerably in recent years, allosteric mechanisms remain difficult to establish because defining changes in protein dynamics is challenging even for small proteins (26). Here, we present hydrogen-deuterium exchange data that suggest the protein samples a larger conformational ensemble upon fructose 1,6-bisphosphate binding. Mapping deuterium exchange to peptides within the protein reveals regions that show significantly altered conformational dynamics upon the binding of fructose

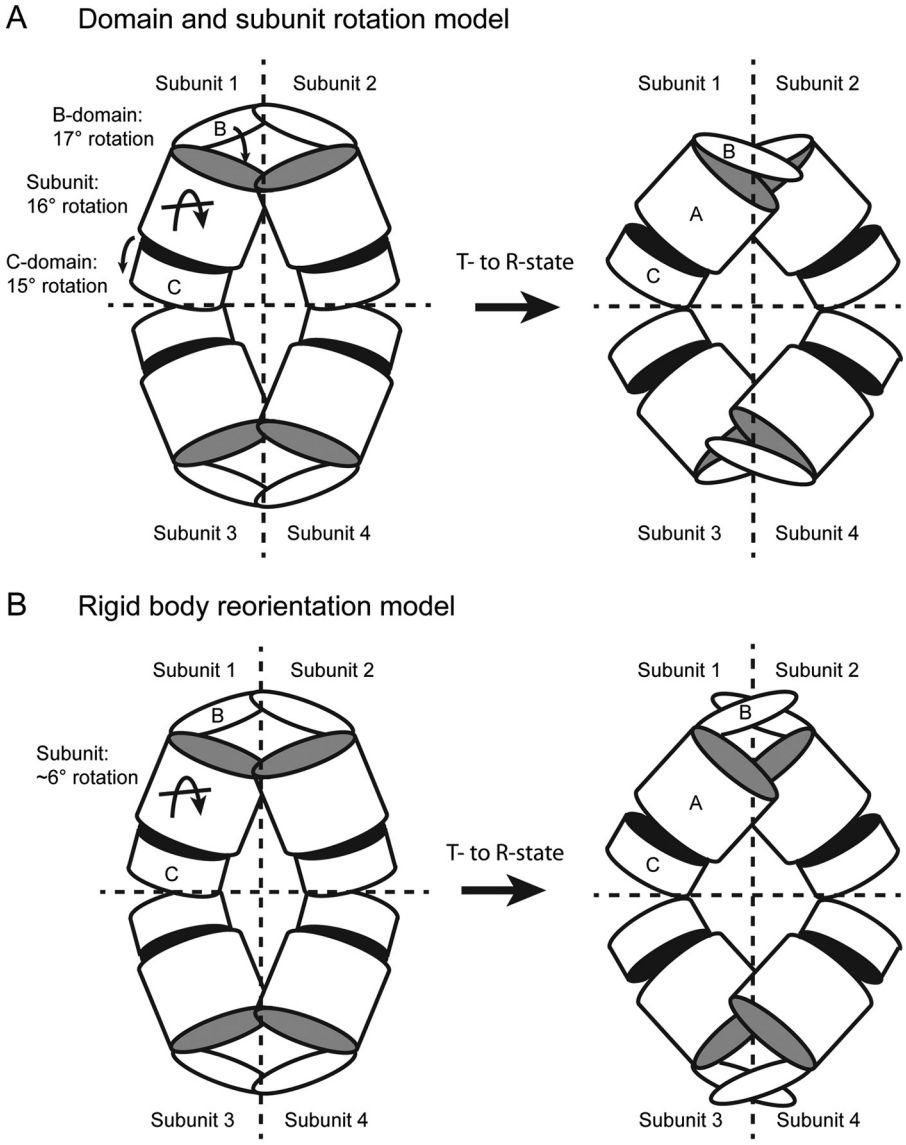

FIGURE 2. **Schematic representation of the two proposed allosteric activation models.** *A*, the "domain and subunit rotation model" proposes that fructose 1,6-bisphosphate binding causes a 16° subunit rotation and rotations of the B- (17°) and C-domains (15°). *B*, the "rigid body rotation model" suggests a ~6–8° symmetrical rigid domain rocking motion of the A/C-domain cores around a pivot point.

1,6-bisphosphate. Based on these dynamic data and further confirmation by mutagenic experiments, we are able to propose a new, detailed mechanism by which fructose 1,6-bisphosphate promotes substrate binding despite the allosteric binding site being 40 Å away from the active site.

Experimental Procedures

Chemicals and Supplies—Pepsin-agarose beads, deuterium oxide (D_2O; 99.99%), ammonium acetate (99.99%), and high purity acetic acid (99.7%) were purchased from Sigma-Aldrich. Fructose 1,6-bisphosphate (Sigma-Aldrich) was prepared in 200 mM ammonium acetate buffer, pH 6.9. Polytetrafluoroethylene tubing (outer diameter, 1/16 inch; inner diameter, 400 μm; and outer diameter, 1/16 inch; inner diameter, 205 μm) was supplied by McMaster Plastics (Scarborough, Ontario, Canada). Standard 1/16-inch fittings were purchased from Upchurch (Oak Harbor, WA). Ultrapure water was generated in house on a Millipore Milli-Q Advantage A10 system.

Cloning of pykF Enzymes—The *pyk*F gene had been cloned into a pBluescript II KS+ vector (23) and was kindly donated by Professor Andrea Mattevi (University of Pavia). In addition to the wild type, four variants of the *pyk*F gene were synthesized commercially by GenScript and supplied in a pBluescript II KS+ cloning vector. The five genes were then digested with SacI and HindIII (New England Biolabs) restriction enzymes and subcloned into the pET30ΔS.E. expression vector (28), purified using an agarose DNA extraction kit (Roche Applied Science), and ligated with T4 DNA ligase at 20 °C for 30 min.

Expression and Purification—The recombinant expression vectors were transformed into chemically competent *E. coli* BL21(DE3) cells for expression and purification.

Purification of wild-type enzyme for hydrogen-deuterium exchange studies was adapted from the procedure used by others (22, 23, 29, 30). Briefly, the procedure involved three purification steps: anion exchange chromatography, hydrophobic interaction chromatography, and size exclusion chromatogra-

phy to obtain pure enzyme as judged by SDS-PAGE. The protein was desalted using a 2-ml Zeba^{TM} spin desalting column (Thermo Scientific) followed by overnight buffer exchange into a 200 mM ammonium acetate buffer, pH 6.9, using a Slide-A-Lyzer Mini dialysis device (10-kDa molecular mass cutoff; Thermo Scientific).

Recombinant wild-type and variant forms were purified in the following way for the mutagenic studies. Crude lysate was loaded onto a HisTrap FF crude 5-ml column (GE Healthcare) pre-equilibrated with buffer A (20 mM Tris, 200 mM KCl, 20 mM imidazole, pH 8). The bound His-tagged protein was eluted with an increasing imidazole concentration as buffer A was replaced with buffer B (20 mM Tris, 200 mM KCl, 500 mM imidazole, pH 8). The fractions containing protein were pooled, and thrombin was added (5 units/mg of protein) for cleavage overnight on a rotation wheel at 4 °C. The cleaved protein was loaded onto a HisTrap FF column, and the flow-through was collected, concentrated, and desalted on a 16/600 Superdex 200 gel filtration column (GE Healthcare) pre-equilibrated with buffer C (10 mM Tris, 2 mM β-mercaptoethanol, 1 mM EDTA, pH 7.5).

Thermal Stability Assays—The unfolding temperatures of the wild-type pyruvate kinase type 1 and four variants (K404A, T405A, Q408A, and L411E) were determined using differential scanning fluorometry following methods adapted from Morgan *et al.* (17). Specifically, 25-μl solutions containing 10× SYPRO Orange (diluted 1:500 in 10 mM Tris, 2 mM, β-mercaptoethanol, 1 mM EDTA, pH 7.5), 0.25 mg/ml protein, and 0.25 mM fructose 1,6-bisphosphate (dissolved in double distilled H_2O) as appropriate were prepared. The samples were heated in an iQ5 real time PCR detection system from 20 to 100 °C with 10-s fluorescence measurements taken in 0.5 °C increments.

Kinetic Analysis—Pyruvate kinase initial rate data were measured using the lactate dehydrogenase-coupled spectrophotometric assay adapted from Valentini *et al.* (30). Enzymatic activity was assayed at 30 °C using varied concentrations of fructose 1,6-bisphosphate, phosphoenolpyruvate, and ADP. Kinetic parameters were determined as follows: titration of phosphoenolpyruvate at a fixed concentration of 4 mM ADP in the absence or presence of 4 mM fructose 1,6-bisphosphate, titration of ADP at a fixed concentration of 4 mM phosphoenolpyruvate in the absence or presence of 4 mM fructose 1,6-bisphosphate, and titration of fructose 1,6-bisphosphate at 1 mM phosphoenolpyruvate and 4 mM ADP. All measurements were performed in duplicate, and the data were fit to the Hill cooperative model (31) to derive V_{max}, $S_{0.5}$, and n_H values.

Microfluidic Device Fabrication—The microfluidic device was constructed as described previously (32, 33). Briefly, the microfluidic channel design was generated in CorelDraw X3 (Corel Co., Ottawa, Ontario, Canada) and lasered onto blank precut polymethyl methacrylate (PMMA)[4] substrate (8.9 × 3.8 × 0.6 cm; Professional Plastics, Fullerton, CA). The design included two input channels for the introduction of reactants, a pepsin digestion chamber (31.5 × 3 mm; 0.5 mm; volume, 47.25 μl), and an output channel. The design was engraved into the PMMA substrate using a 30-watt CO_2 Versa-Laser engraving device (Universal Laser, Scottsdale, AZ).

A protein microfluidic channel was created as described previously (34) by passing a polyimide-coated glass capillary (outer diameter, 153 μm; inner diameter, 75 μm; Polymicro Technologies, Phoenix, AZ) through a 12-cm-long metal capillary (outer diameter, 318 μm; inner diameter, 158.75 μm). The distal end of the glass capillary was sealed with fused silica by cutting at high laser power, and a notch was cut 2 mm from the sealed end. The proximal end of the mixing channel was pressure-fit into polytetrafluoroethylene tubing and connected to a three-way T-union. The distal end of the glass capillary was then pulled back until it was flush with the metal capillary and soldered into one of the input channels on the PMMA substrate, which created the entrance for both the protein and D_2O. Two metal capillaries (outer diameter, 400 μm; inner diameter, 200 μm; Small Parts, Inc., Miramar, FL) were soldered into the second input channel for supplying the acid quenching solution (12.5% acetic acid, pH 2.3) and the output channel, which served as the electrospray ionization source for direct coupling to the MS. The engraved PMMA substrate was lined with a piece of silicon rubber to create a liquid-tight seal around the reaction well. Pepsin-agarose (~15 mg) was evenly spread over the digestion "well" using 1 M HCl. A second blank PMMA substrate was used as a cover to seal the device. The chip and cover were placed in a custom-built clamp (LAC Machine and Tooling Limited, Ontario, Canada) to pressure-seal the microfluidic device. The reactants were then supplied into the input channels of the device using Harvard syringes through polytetrafluoroethylene tubing using automated syringe infusion pumps (Harvard Apparatus, Holliston, MA).

Time-resolved Electrospray Ionization Mass Spectrometry-coupled Proteolytic Experiments—The microfluidic chip was interfaced with a modified QSTAR Elite hybrid quadrupole time-of-flight (QqTOF) mass spectrometer (Sciex, MDS Analytical Technologies, Concord, Ontario, Canada). The instrument was operated in positive ion mode with optimal running conditions of 4600–5000-V source voltage, 10-V declustering potential, and 100-V focusing potential. Spectra were acquired over the range of 400–1500 m/z with a scanning rate of 1 s^{-1}.

Hydrogen-deuterium exchange experiments were carried out at 20 °C in triplicate. The purified protein (38 μM in 200 mM ammonium acetate, pH 6.9) was introduced into the glass capillary of the mixing device at a flow rate of 1 μl/min, whereas the D_2O was introduced into the outer metal capillary at a flow rate of 3 μl/min using Harvard 11+ infusion pumps. Where appropriate, the enzyme was preincubated with 2 mM fructose 1,6-bisphosphate (10 times the K_D of 0.2 mM (30, 35–37)) to ensure the saturation of the allosteric binding sites. The fluids followed a laminar flow pattern until they reached the notch in the glass capillary at which point they were combined and mixed. The reaction time was adjusted by changing the position of the mixing capillary within the channel; labeling times of 59 ms to 1 s were used in the experiment. Pulling the mixing glass capillary back increased the dead space after mixing, thus increasing the reaction time. Reaction labeling was immediately quenched by reduction of pH to ~2.6 by using a 12.5% acetic acid solution, pH 2.3 (8 μl/min), creating a 75:25 H_2O/D_2O mixture. The

[4] The abbreviation used is: PMMA, polymethyl methacrylate.

protein-D_2O-acid mixture was digested across the pepsin-agarose beads of the digestion well for rapid digestion with minimal back-exchange. Voltage (4600–5000 V) was applied to the electrospray ionization source capillary creating a gas "spray" of peptides that was detected on the QqTOF MS. The samples were scanned over the 400–1500 m/z range.

Data Analysis—All MS spectra analyses were carried out as described previously (38) on mMass software, version 5.5 (39). Peptide identification was performed using a FindPept tool on the ExPASy proteomic server (Swiss Institute of Bioinformatics, Basel, Switzerland) in conjunction with collision-induced dissociation to identify any ambiguous peptides. The amount of deuterium exchange was computed using software for isotropic distribution analysis developed in house and normalized to the maximum deuterium exchange of 75%. Hydrogen-deuterium exchange kinetic data were fitted using single exponential non-linear regression analysis ($y = y_0 + a(1 - e^{-kt})$) and normalized in OriginPro (v8.5.1). Protein structures were rendered using PyMOL (The PyMOL Molecular Graphics System, Version 1.5.0.4, Schrödinger, LLC).

Results and Discussion

Proteins exist as an ensemble of conformers, and conformational sampling allows proteins to fluctuate between different conformers (40–42). The lowest energy state is the most favorable; thus, a greater proportion of the population will exist in this state (24, 43). In theory, all possible conformational states of a protein can be mapped and described by an energy landscape (24, 44), although in practice detecting high energy conformers is more challenging because of their small number in the population and transient nature. In the dynamic view of allostery, the binding of the allosteric modulator remodels the energy landscape and triggers a shift in the relative occupancy of states in the conformational ensemble (24, 26, 42); the conformation that represents the lowest energy state is changed, although many conformers may still be sampled. Importantly, this shift increases how often a given (activated or inhibited) state is sampled (24, 26, 44). For example, the binding of reduced nicotinamide adenine dinucleotide phosphate increases how often dihydrofolate reductase samples the active "R-state" (27, 45).

Fructose 1,6-Bisphosphate Binding Causes an Increase in Global Protein Flexibility—To gauge changes in global conformational dynamics, global hydrogen-deuterium exchange was measured as a time course (14 ms to 1.5 s) for *E. coli* pyruvate kinase type 1 with and without its allosteric activator, fructose 1,6-bisphosphate. The data were fitted to an exponential function, generating a kinetic plot of overall protein deuterium exchange (Fig. 3). Increases in deuterium exchange characteristically result from intermittent loss of hydrogen bonds within and between secondary structure elements due to changes in structure or conformational flexibility, leading to increased solvent access associated with destabilization of secondary structure and tertiary structure. By the same token, decreases in deuterium exchange typically result from stable hydrogen bond formation within secondary structure elements and decreased solvent accessibility.

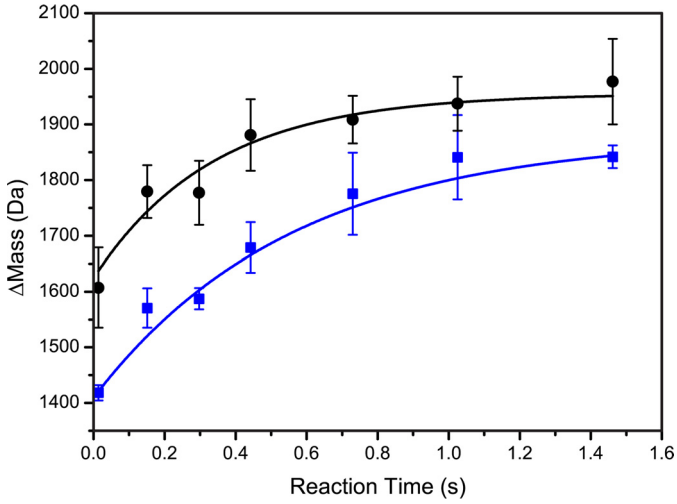

FIGURE 3. **Global deuterium exchange kinetics for *E. coli* pyruvate kinase type 1.** The global hydrogen deuterium exchange experiment was measured in the absence (■) and presence (●) of fructose 1,6-bisphosphate, providing initial exchange rates of 1.9 ± 0.5 and 2.9 ± 0.8 s^{-1}, respectively. Kinetic data were fitted using single exponential non-linear regression analysis ($y = y_0 + a(1 - e^{-kt})$). The first time point is at 14 ms. The binding of fructose 1,6-bisphosphate increased the total amount of deuterium exchanged from 1884 (without ligand) to 1966 Da (with ligand). This Δmass is the amount of deuterium exchanged into the protein exclusive of the mass of fructose 1,6-bisphosphate. *Error bars* represent S.E. of three replicates.

The global hydrogen-deuterium exchange kinetic plot (Fig. 3) reveals that when fructose 1,6-bisphosphate is present the enzyme has a higher amplitude of deuterium exchange (~Δ1966 Da), which is evident in the increased change in mass seen at 1–1.5 s. In the absence of fructose 1,6-bisphosphate, the amplitude is ~Δ1884 Da. Moreover, we note that there is a difference in the burst phase (0–14 ms) between the differently treated proteins. This is consistent with a globally more dynamic protein that can exchange deuterium more readily. From this, we infer that the binding event causes a shift toward a more unstructured, heterogeneous protein.

Not only was there a change in the amount of deuterium taken up by the protein on the time-resolved electrospray ionization mass spectrometry time scale (milliseconds to seconds), but the rate of exchange was also augmented upon fructose 1,6-bisphosphate binding, corresponding to an increase from 1.9 ± 0.5 to 2.9 ± 0.8 s^{-1}. This is also consistent with activator binding increasing the globally averaged dynamic conformational sampling the protein is undergoing over time: that is, fructose 1,6-bisphosphate increases not only the extent of conformational space being sampled but also how "fast" the protein explores conformational space (46).

To corroborate this global time-resolved electrospray ionization mass spectrometry experiment, we measured the thermal stability of the wild-type enzyme in the absence and presence (0.25 mM) of fructose 1,6-bisphosphate. We found that fructose 1,6-bisphosphate decreases the thermal stability by ~5 °C from 54.3 ± 0.3 (S.D.) to 49.7 ± 0.3 °C. This had been previously observed for the *E. coli* pyruvate kinase type 1 enzyme (30) but is in contrast to the *T. cruzi* and *T. brucei* pyruvate kinase enzymes where fructose 1,6-bisphosphate increases the thermal stability (10). Taken together, these data suggest that fructose 1,6-bisphosphate binding to the allosteric domain causes a

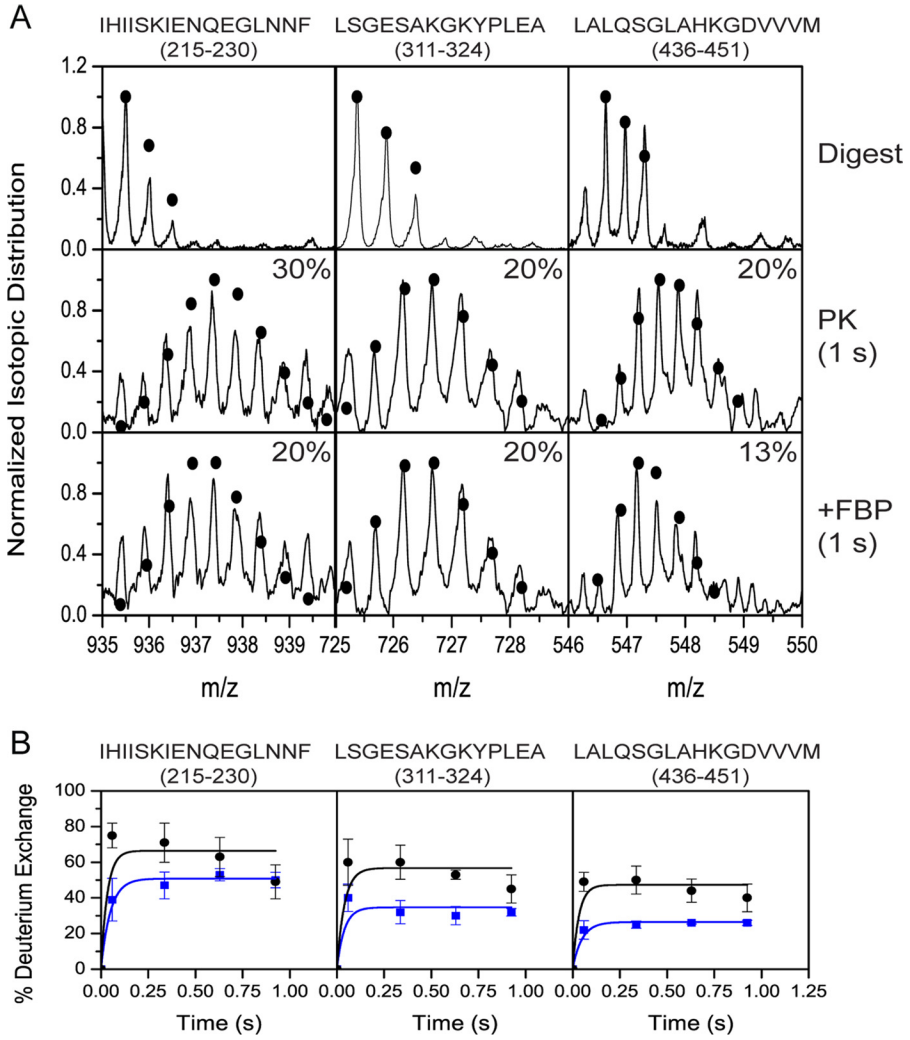

FIGURE 4. **Analysis of site-specific hydrogen-deuterium exchange analysis.** *A*, representative spectra for peptides derived from pyruvate kinase for non-deuterated pyruvate kinase (*top row*), deuterated pyruvate kinase from 1-s labeling time (*second row*), and deuterated pyruvate kinase with bound fructose 1,6-bisphosphate from 1-s labeling time (*third row*). The raw spectra illustrate the observed shifts in isotopic distribution following hydrogen-deuterium exchange, and *black circles* denote the theoretical isotopic distribution generated using FORTRAN (developed in the Wilson Laboratory, York University). The raw percentage of deuterium exchange for the illustrated replicate is indicated on each spectra. *B*, hydrogen-deuterium exchange kinetic plots of representative peptides for pyruvate kinase type 1 in the absence (■) and presence (●) of fructose 1,6-bisphosphate (*FBP*). Data represent an average of triplicate runs (*error bars* denote S.E.). Kinetic data were fitted using single exponential non-linear regression analysis ($y = y_0 + a(1 - e^{-kt})$).

shift toward a globally more unstructured and dynamic ensemble of conformations. This may also explain our (and others' (8)) observation that treating crystals of *E. coli* pyruvate kinase type 1 with fructose 1,6-bisphosphate results in crystal cracking and the lack of conditions for co-crystallization.

Localized Changes in Deuterium Exchange Reveal Regions with Altered Conformational Flexibility—To provide detailed information on regions of the protein where conformational flexibility significantly changes upon fructose 1,6-bisphosphate binding, enzyme that was premixed with deuterium (59 ms to 1 s) was digested using pepsin, and we determined the amplitude of deuterium exchange on individual peptides over this time period. Digestion of pyruvate kinase type 1 was effective given the size of the protein, resulting in a 64% sequence coverage corresponding to 36 distinctive peptides and an average spatial resolution of 10 amino acid residues. Typical raw hydrogen-deuterium exchange mass spectrometry data of representative peptides (Fig. 4*A*) demonstrate the shift in the mass envelope caused by differences in deuterium exchange of unbound and bound pyruvate kinase peptides. Kinetic hydrogen-deuterium exchange profiles of the representative peptides were fit to a single exponential expression to illustrate a change in peptide deuterium exchange as a function of labeling time (Fig. 4*B*).

We then mapped the percentage of deuterium exchange for each peptide onto the pyruvate kinase structure to illustrate regions that have significant changes in local backbone dynamics (Fig. 5; the color spectrum indicates the level of exchange: *blue* to *red*, low to high exchange, respectively). Qualitatively, the protein in the absence of fructose 1,6-bisphosphate shows generally low exchange of deuterium (20–60%), commensurate with a stable, globular structure. In particular, the peptides close to the tetrameric interfaces (A/A′, peptide 291–294; and C/C′, peptide 452–467) show low exchange, which is consistent with our previous work demonstrating that pyruvate kinase type 1 is a very stable tetramer ($K_D^{4\text{-}1} < 10$ nM) (35).

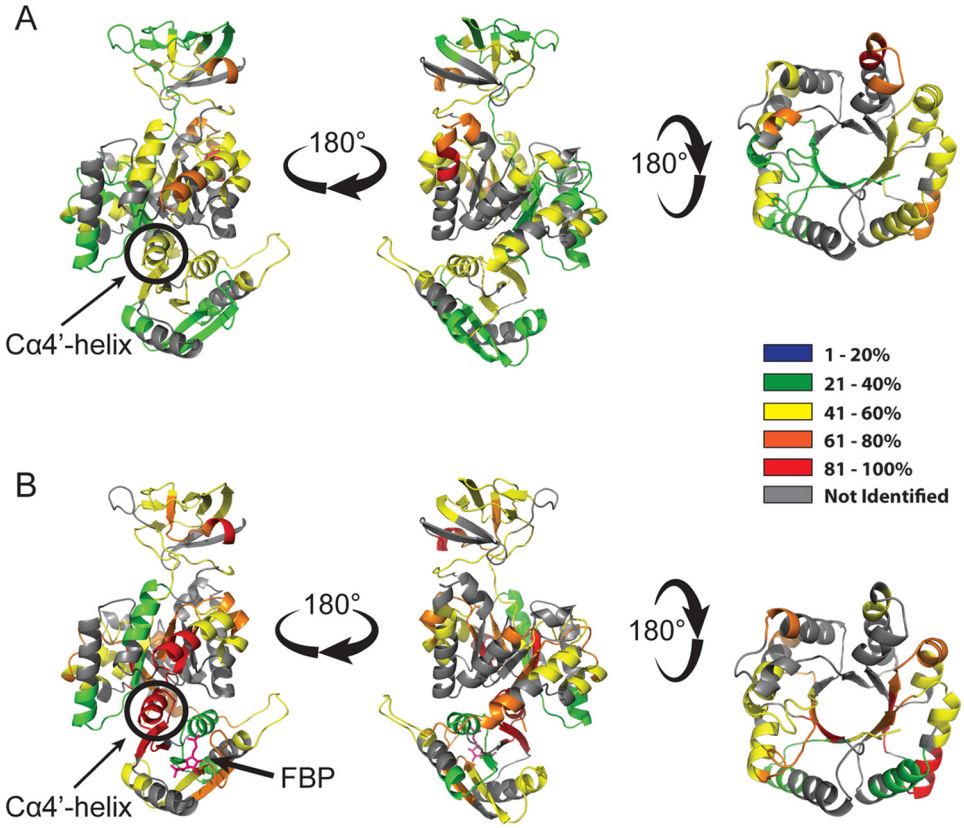

FIGURE 5. **Average deuterium exchange mapped and color-coded onto the *E. coli* pyruvate kinase structure (Protein Data Bank code 4YNG (53)).** *A*, unbound pyruvate kinase, viewing both sides of the subunit and looking down the $(\beta/\alpha)_8$-barrel. *B*, pyruvate kinase with the allosteric activator fructose 1,6-bisphosphate (*FBP*) (*magenta*) modeled into the structure (based upon Protein Data Bank code 1A3W), viewing both sides of the subunit and looking down the $(\beta/\alpha)_8$-barrel. The *gray* regions were not identified in the hydrogen-deuterium exchange experiment. The Aα4′-helix, residues 398–408, is *circled* in *black*. Only peptides that are identified in both experiments (with and without fructose 1,6-bisphosphate) are displayed.

Moreover, the peptides at the A/C interdomain interface (peptides 398–408 and 409–419; Fig. 5, *circled*) have relatively low deuterium exchange (47 and 56%) compared with the same peptide in the presence of fructose 1,6-bisphosphate (87 and 95%).

When mapping the degree of exchange in peptides derived from protein pretreated with fructose 1,6-bisphosphate and comparing this with the unbound peptides, it is evident that the pattern of exchange is different (Fig. 5, *A* and *B*). Fig. 6*A* shows only those peptides that exhibited a significant change in absolute deuterium exchange (>15% absolute difference) when comparing peptides derived from unbound enzyme with those from fructose 1,6-bisphosphate-bound enzyme. To permit straightforward interpretation of the data, the absolute changes are noted only as an increase or decrease in exchange (Fig. 6*B*). The percentage of change in deuterium exchange upon fructose 1,6-bisphosphate binding was then mapped to the structure to highlight regions of the protein that exhibited significant changes in backbone deuterium exchange (Fig. 6*C*). Clearly, there are regions that show significant changes, which we address in the sections below.

Dynamic Changes to the Allosteric Domain upon Fructose 1,6-Bisphosphate Binding—We first examined the allosteric binding domain to assess how fructose 1,6-bisphosphate binding affects its conformational flexibility. From Fig. 6, fructose 1,6-bisphosphate binding results in clear changes in deuterium exchange in the allosteric C-domain. Because a structure of *E. coli* pyruvate kinase type 1 with bound fructose 1,6-bisphosphate is not available, we have modeled fructose 1,6-bisphosphate binding to the allosteric binding domain using overlays with the *S. cerevisiae* pyruvate kinase structure (11) (Fig. 7, *A* and *B*). For *S. cerevisiae* pyruvate kinase, fructose 1,6-bisphosphate binding in the allosteric site is facilitated by residue Arg^{459}, forming a strong electrostatic interaction with the 1′-phosphate group of fructose 1,6-bisphosphate. In addition, the 6′-phosphate makes a series of hydrogen bonds with side chains from the sequence Ser^{402}-Thr-Ser-Gly-Thr-Thr^{407} (Thr^{378}-Gln-Gly-Gly-Lys^{382} are the equivalent residues in *E. coli* pyruvate kinase type 1), and the sugar ring of the fructose 1,6-bisphosphate forms interactions with residues Gln^{483} and His^{491}. Moreover, chemical modification of *E. coli* pyruvate kinase type 1 identifies Lys^{382} (equivalent to Thr^{406} in *S. cerevisiae* pyruvate kinase) as important for fructose 1,6-bisphosphate binding, providing some evidence that the allosteric binding site is located in a pocket similar to that of *S. cerevisiae* pyruvate kinase (11).

The binding site for fructose 1,6-bisphosphate in the allosteric domain shows key changes in conformational flexibility. Assuming fructose 1,6-bisphosphate binds in the same pocket and in a similar orientation, ligand binding requires a displacement of surface-accessible water molecules and a change in the hydrogen bonding network of the pocket, including residues of

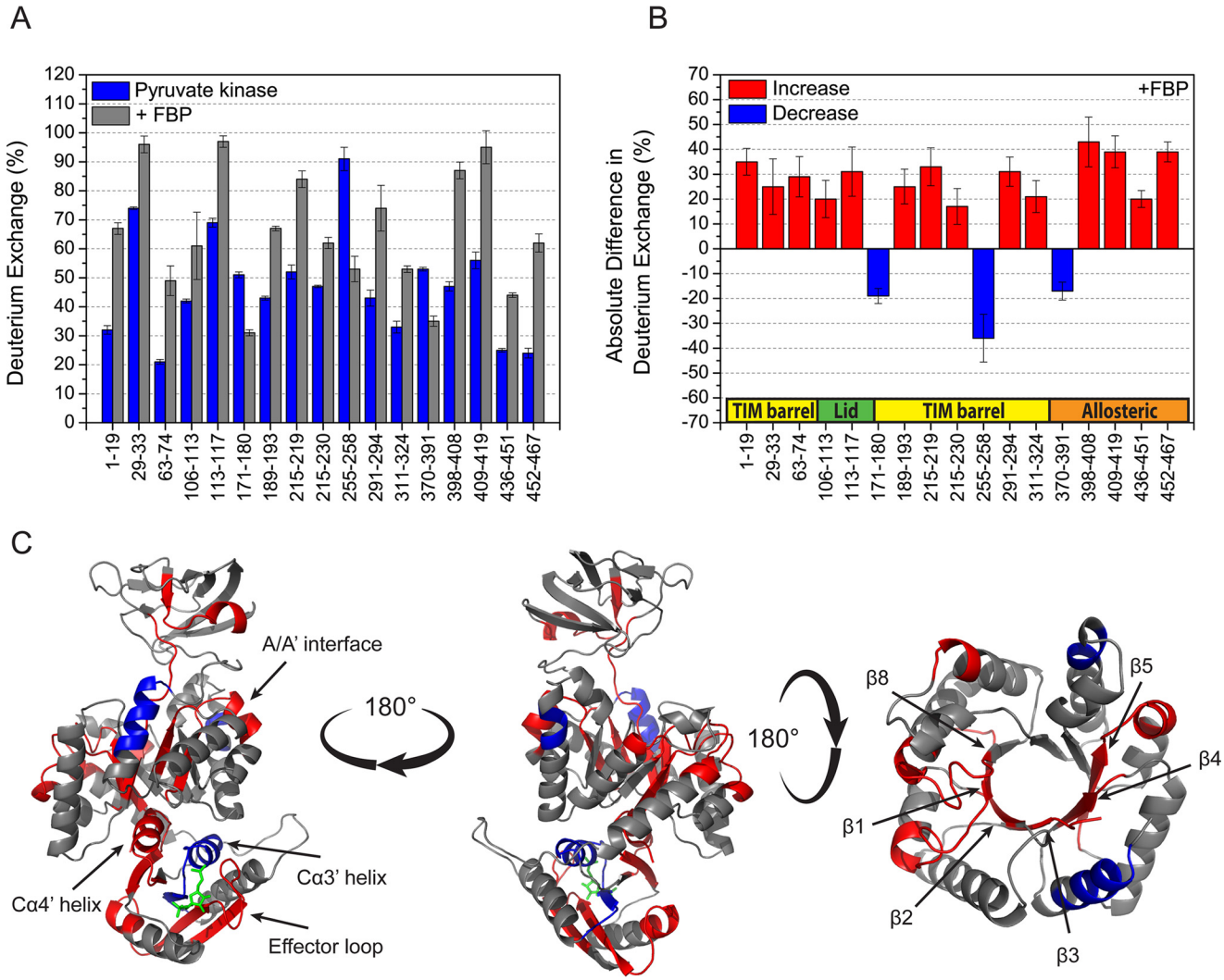

FIGURE 6. **Change in average deuterium exchange between the unbound and bound pyruvate kinase peptides.** *A*, amount of deuterium exchange in peptides derived from unbound (*blue*) and fructose 1,6-bisphosphate-bound (*FBP*) (*red*) pyruvate kinase. Only peptides showing a significant difference (>15% absolute difference in normalized deuterium exchange) are plotted. *B*, absolute differences (>15%) in deuterium exchange are plotted as an increase (*red*) or a decrease in exchange (*blue*) in the presence of fructose 1,6-bisphosphate. *C*, absolute differences (>15%) are mapped onto the pyruvate kinase subunit as an increase (*red*) or a decrease in exchange (*blue*). The allosteric activator fructose 1,6-bisphosphate (*green stick*) has been modeled into the structure to show the binding position and is based upon the structure of *S. cerevisiae* pyruvate kinase (Protein Data Bank code 1A3W). Data represent an average of triplicate runs, and *error bars* represent the S.E.

the Cα3′- and Cα4′-helices and the effector loop (Fig. 7*C*), so we expected to find changes to the backbone flexibility in these regions. We note first that the surface that binds fructose 1,6-bisphosphate has decreased exchange, consistent with fructose 1,6-bisphosphate binding decreasing the availability of amides and preventing exchange. In addition, there is a large increase in deuterium exchange for the peptide containing the effector loop, residues 452–467 (Fig. 6*C*). The effector loop is at the suspected activator binding site, and it shows a 38% increase in deuterium exchange. It has been implicated as the fructose 1,6-bisphosphate binding loop (10, 17), and in the unbound state it is located very near the position of suspected fructose 1,6-bisphosphate binding. One interpretation of our result is that fructose 1,6-bisphosphate binding pushes the enzyme toward a conformational state that favors the effector loop positioned to the side. Fig. 7*A* shows the position of the effector loop when fructose 1,6-bisphosphate is bound in the *S. cerevisiae* structure, whereas Fig. 7*B* shows the effector loop position in the absence of fructose 1,6-bisphosphate (*E. coli* pyruvate kinase with fructose 1,6-bisphosphate modeled into the binding site from Protein Data Bank code 1A3W), illustrating the change in conformation for this loop that may occur.

The neighboring Cα3′-helix (residues 370–391) has a 17% decrease in deuterium exchange (Fig. 6, *B* and *C*). The decrease in dynamics for the Cα3′-helix may be due to hydrogen bonding with fructose 1,6-bisphosphate, decreasing the number of amide hydrogen atoms available for exchange. In the *S. cerevisiae* structure (Protein Data Bank code 1A3W), the 6′-phosphate of fructose 1,6-bisphosphate hydrogen bonds with Thr^{407} of the Cα3′-helix (11). That the 382 variant, which precedes the Cα3′-helix of *E. coli* pyruvate kinase type 1, results in a 70-fold decrease in fructose 1,6-bisphosphate binding affinity (30) supports the assumption that this helix also binds the allosteric activator in the *E. coli* enzyme. Hydrogen bond formation with fructose 1,6-bisphosphate may cause a reorientation of residue Gln^{379}, weakening its interactions with residues Asn^{402} and

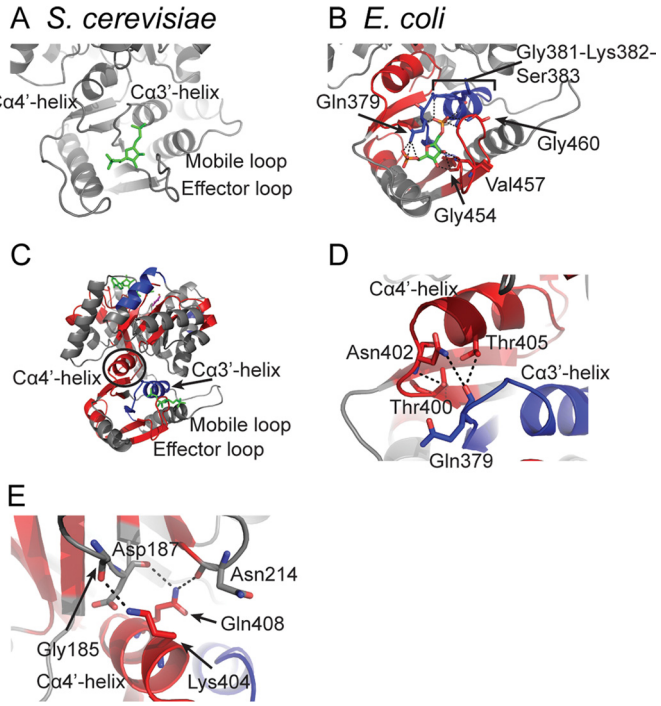

FIGURE 7. **Dynamic changes to the pyruvate kinase allosteric domain.** *A*, *S. cerevisiae* allosteric domain with fructose 1,6-bisphosphate bound (*green*) (Protein Data Bank code 1A3W). *B*, *E. coli* type 1 pyruvate kinase allosteric domain with fructose 1,6-bisphosphate (*green*) modeled from Protein Data Bank code 1A3W into the binding site showing proposed interactions. *C*, $(\beta/\alpha)_8$-barrel and allosteric domains with the Cα4′-helix *circled*. *D*, interactions between Cα3′- and Cα4′-helices. *E*, interactions between the Cα4′-helix and loops $\alpha_3\beta_3$ and $\alpha_4\beta_4$. Significant changes (>15% absolute difference) in deuterium exchange are mapped onto the pyruvate kinase subunit as an increase (*red*) or a decrease in exchange (*blue*). Relevant residues are shown as *sticks*, and key regions of the protein have been labeled. Interactions are displayed as *dashed lines*.

Thr^{405} of the Cα4′-helix (Fig. 7*D*). The mutagenic study at Lys^{382} and the significant decrease in conformational flexibility we observed collectively support the concept that the Cα3′-helix is directly involved in interactions with fructose 1,6-bisphosphate and important for communicating the allosteric signal to the Cα4′-helix.

Significantly, fructose 1,6-bisphosphate binding also causes destabilization of the interdomain interface that links the allosteric domain (C-domain) and the $(\beta/\alpha)_8$-barrel (A-domain) within the monomer (Fig. 7). Our dynamic data, when mapped onto the structure, suggest that the interactions between the allosteric domain and the A-domain are largely mediated by the Cα4′-helix of the allosteric domain (*circled* in Figs. 5*B* and 7*C*) and the N-terminal loops of the $(\beta/\alpha)_8$-barrel. The binding of fructose 1,6-bisphosphate causes a 40% increase in deuterium exchange of an α-helix (Cα4′-helix) motif that forms the interface between the $(\beta/\alpha)_8$-barrel (A-domain) and the allosteric domain (C-domain). This strongly suggests that it may play an important part in the transition between inactive and active state populations. This result is inconsistent with the *L. mexicana* and *T. cruzi* pyruvate kinase crystal structures (10, 47), which show a rigid body rocking of the A/C-core domains, and temperature factor analysis of these structures does not suggest that fructose 1,6-bisphosphate binding affects the mobility of the A/C interdomain interface. Our result is, however, consistent with the model put forward by Mattevi *et al.* (8), who reasoned that the A/C-domains were altered based on the non-allosteric rabbit M1 structure.

Mutational analysis of residues at the A/C interdomain interface is consistent with the dynamic changes that we observed. First, Valentini *et al.* (30) created variant enzymes to perturb salt bridges between the A- and C-domains. They created the substitutions K413Q, which is at the end of the Cα4′-helix, and R271L, which sits above the Cα3′-helix, resulting in severely altered functional behaviors compared with the wild-type enzyme. Lys^{413} is positioned on a peptide that has increased deuterium uptake in the presence of fructose 1,6-bisphosphate. Importantly, the K413Q amino acid substitution induced activation of the enzyme in the absence of fructose 1,6-bisphosphate, shown by a left shift of the phosphoenolpyruvate saturation curve ($S_{0.5}$ for phosphoenolpyruvate binding decreased in K413Q compared with wild type) (30). Similar work in *Bacillus stearothermophilus* pyruvate kinase where the equivalent residue is substituted (W466Y) also demonstrated activation of the variant enzyme in the absence of the allosteric activator (48). In contrast, the R271L amino acid substitution resulted in a 5-fold increase in $S^{0.5}$ for fructose 1,6-bisphosphate binding as well as a right shift of the phosphoenolpyruvate saturation curve in the absence of fructose 1,6-bisphosphate, suggesting that it does affect the Cα3′-helix, which binds fructose 1,5-bisphosphate. Thus, these two variants validate the significance of the A/C interdomain salt bridges for allosteric signal transfer between allosteric and catalytic domains, consistent with our hydrogen-deuterium exchange studies.

Next, we created four *E. coli* pyruvate kinase variants at the Cα4′-helix to probe the role of hydrogen bonds within the region that bridges the A- and C-domains on the allosteric mechanism. Thr^{405} interacts with the end of the Cα3′-helix, whereas Lys^{404} and Gln^{408} form hydrogen bonds with residues at the bottom of the A-domain, and Leu^{411} sits in a hydrophobic pocket at the N-terminal end of the $(\beta/\alpha)_8$-barrel. Kinetic analysis of these variants is presented in Table 1.

The substitution of Thr^{405} to alanine results in a 5-fold increase in the $S_{0.5}$ for fructose 1,6-bisphosphate from 0.006 ± 0.001 mM for the wild-type enzyme to 0.029 ± 0.009 mM for the T405A variant. This is consistent with the proposed interaction of the Cα4′- and Cα3′-helices whereby fructose 1,6-bisphosphate binding alters the hydrogen bonding pattern between Gln^{379} and the Cα4′-helix.

The Q408A variant, which bridges the A- and C-domains, shows a significant right shift of both ADP and phosphoenolpyruvate saturation curves in the presence of fructose 1,6-bisphosphate. In addition, the enzyme is catalytically compromised in the absence of fructose 1,6-bisphosphate (k_{cat} = 95 ± 3 s^{-1} compared with wild-type k_{cat} = 216 ± 4 s^{-1}). Thus, the mechanism of allostery appears to be changed: for this variant, fructose 1,6-bisphosphate also affects the maximal rate (k_{cat} = 95 ± 3 s^{-1} in the absence but 283 ± 30 s^{-1} in the presence of fructose 1,6-bisphosphate). Interestingly, Q408A has decreased thermostability (47.5 ± 0 °C), which is further destabilized 10 °C by fructose 1,6-bisphosphate (37.3 ± 0.3 °C). This variant, which bridges the Cα4′-helix with the A-domain via the main chains of Ala^{187} and Asp^{214} and the side chain of His^{216}, sug-

TABLE 1

Kinetic parameters for variant enzymes with substitutions in the Cα4′-helix

The variants were designed to probe the role of the hydrogen bonding network in this helix with the Cα3′-helix that binds to fructose 1,6-bisphosphate (T405A) and the interface with the A-domain (L404A and G408A). Pyruvate kinase initial rate data were measured using the lactate dehydrogenase-coupled spectrophotometric assay adapted from Valentini *et. al.* (30). All measurements were performed in duplicate, and the data were fit to the Hill cooperative model (31) to derive V_{max}, $S_{0.5}$ and n_H values.

Phosphoenolpyruvate titration (ADP fixed at 4 mM)						
	With fructose-1,6-bisphosphate (4 mM)			**w/o fructose-1,6-bisphosphate**		
	k_{cat} (s^{-1})	$S_{0.5}$ (mM)	n_H	k_{cat} (s^{-1})	$S_{0.5}$ (mM)	n_H
Wild-type	271 ±4	0.083 ±0.005	1.12 ±0.07	216 ±4	1.34 ±0.03	3.5 ±0.2
Lys404Ala	292 ±6	0.071 ±0.005	1.15 ±0.08	259 ±16	1.4 ±0.1	2.9 ±0.4
Thr405Ala	299 ±8	0.061 ±0.006	1.2 ±0.1	135 ±10	1.9 ±0.1	3.2 ±0.4
Gln408Ala	217 ±7	0.4 ±0.2	0.59 ±0.09	95 ±3	1.69 ±0.05	4.5 ±0.5
ADP titration (phosphoenolpyruvate fixed at 4 mM)						
	With fructose-1,6-bisphosphate (4 mM)			**w/o fructose-1,6-bisphosphate**		
	k_{cat} (s^{-1})	$S_{0.5}$ (mM)	n_H	k_{cat} (s^{-1})	$S_{0.5}$ (mM)	n_H
Wild-type	297 ±8	0.55 ±0.04	1.27 ±0.07	226 ±4	0.40 ±0.02	1.30 ±0.06
Lys404Ala	303 ±7	0.53 ±0.03	1.30 ±0.07	276 ±22	0.7 ±0.1	1.0 ±0.1
Thr405Ala	329 ±6	0.41 ±0.02	1.29 ±0.06	261 ±10	0.39 ±0.04	1.2 ±0.1
Gln408Ala	283 ±30	2.2 ±0.5	1.00 (fixed)	96 ±2	0.41 ±0.03	1.28 ±0.08

Fructose-1,6-bisphosphate titration (ADP fixed at 4 mM, phosphoenolpyruvate fixed at 1 mM)			
	V_{max} (U/mg)	$S_{0.5}$ (mM)	n_H
Wild-type	177 ±6	0.006 ±0.001	0.8 ±0.1
Lys404Ala	225 ±16	0.003 ±0.001	0.4 ±0.1
Thr405Ala	321 ±37	0.029 ±0.009	0.6 ±0.3
Gln408Ala	101 ±7	0.010 ±0.003	0.6 ±0.1

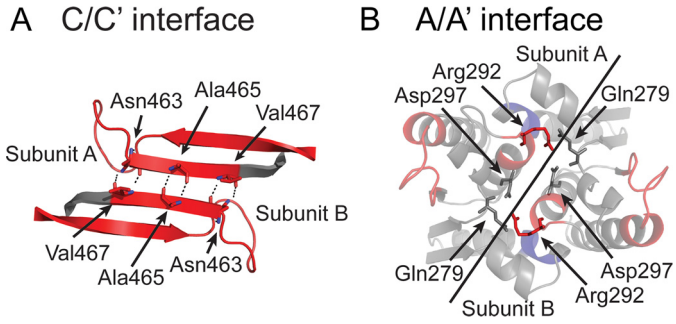

FIGURE 8. **Changes in conformational flexibility within the C/C′ and A/A′ tetrameric interfaces.** Changes in deuterium exchange are mapped onto the *E. coli* pyruvate kinase type 1 structure highlighting exchange changes at the C/C′ interface (*A*) (interactions are shown as *dashed lines*) and A/A′ interface (*B*). Relevant residues are displayed as *sticks* and labeled.

gests clear connections between the A- and C-domains and is consistent with a destabilizing role for the Cα4′-helix but suggests that the level of destabilization is carefully tuned for activation.

The substitution of Lys^{404} with alanine resulted in no change in function, suggesting that this residue plays either a minor or no role in the allosteric mechanism. The introduction of a negative charge to the hydrophobic $(\beta/\alpha)_8$-barrel in L411E resulted in an inactive enzyme and an extremely low unfolding temperature ($T_m \sim 23$ °C), suggesting that amino acid substitutions at the A/C domain interface can destabilize the protein.

To summarize, hydrogen-deuterium exchange studies suggest that fructose 1,6-bisphosphate binding results in large changes in conformational flexibility of key elements within the allosteric domain. First, the effector loop, which in the unbound pyruvate kinase type 1 structure lies across the fructose 1,6-bisphosphate binding site, has increased conformational flexibility, consistent with its displacement upon binding. Second, the Cα3′-helix has decreased conformational flexibility, consistent with fructose 1,6-bisphosphate binding to this helix (Fig. 7*B*), as seen in the *S. cerevisiae* structure. Finally, the Cα4′-helix has increased conformational flexibility (Fig. 7*D*), which we propose is due to weakening interactions between the Cα3′- and Cα4′-helices as the Cα3′-helix binds fructose 1,6-bisphosphate (Fig. 7*D*). This is corroborated by mutagenic data. Substitution of Lys^{413} with alanine at the end of the Cα4′-helix breaks a salt bridge between the A- and C-domains and results in enzyme activation. R271L, which sits above the Cα3′-helix, affects both phosphoenolpyruvate and fructose 1,6-bisphosphate binding, consistent with a key role of the Cα3′-helix in the allosteric mechanism. Disruption of hydrogen bonds within the Cα4′-helix by substitutions at positions Thr^{405}, which interacts with the end of the Cα3′-helix, and Gln^{408}, which interacts with residues at the bottom of the A-domain, results in disruption of fructose 1,6-bisphosphate binding and altered catalysis. Substitution of Leu^{411} with glutamate suggests that changes at this interface can be destabilizing.

The Tetrameric A/A′ and C/C′ Interfaces Are Also Altered upon Fructose 1,6-Bisphosphate Binding—The tetrameric C/C′ interface that is formed by the allosteric domains shows significantly increased conformational flexibility upon fructose 1,6-bisphosphate binding, suggesting that the β-strand (Cβ5′-strand; residues 463–470) that forms this interface is destabilized. Fig. 8*A* shows the C/C′ interface interactions in the unbound *E. coli* pyruvate kinase type 1. These interactions include hydrogen bonds between residues Ala^{465} and $Ala^{465'}$, Val^{467} and $Asn^{463'}$, and Asn^{463} and $Val^{467'}$. Fructose 1,6-bisphosphate binding causes a 38% increase in deuterium exchange in the peptide that includes this strand.

Although peptide coverage across the A/A′ interface is poor (7 of 26 residues in the fructose 1,6-bisphosphate-unbound monomer are within peptides that could be detected in both samples), several peptides show altered deuterium exchange (Fig. 8*A*). The peptide containing residues 291–294 has an increase in deuterium exchange (difference of +31%) and is less structured. In contrast, the peptide containing residues 255–258, which is close to the A/A′ interface, has decreased exchange (difference of −38%) and is, therefore, significantly more structured upon fructose 1,6-bisphosphate binding.

Our deuterium exchange data support an allosteric mechanism whereby fructose 1,6-bisphosphate binding destabilizes and decouples the subunits at the tetrameric interfaces to remove phosphoenolpyruvate cooperation between active sites (homotropic activation). This finding is corroborated by mutagenic studies from two groups, Lovell *et al.* (49) and Fenton and Blair (36), who both created pyruvate kinase variants with amino acid substitutions at the tetrameric interfaces.

First, Fenton and Blair (36) generated the E392A pyruvate kinase variant at the C/C interface, resulting in complete loss of homotropic activation by phosphoenolpyruvate, suggesting that in yeast the active sites communicate through this interface. Moreover, Lovell *et al.* (49) propose that the equivalent A/A interface residue of *E. coli* pyruvate kinase Gln^{279} in *B. stearothermophilus* pyruvate kinase is important in coupling phosphoenolpyruvate binding with cooperative and allosteric functions.

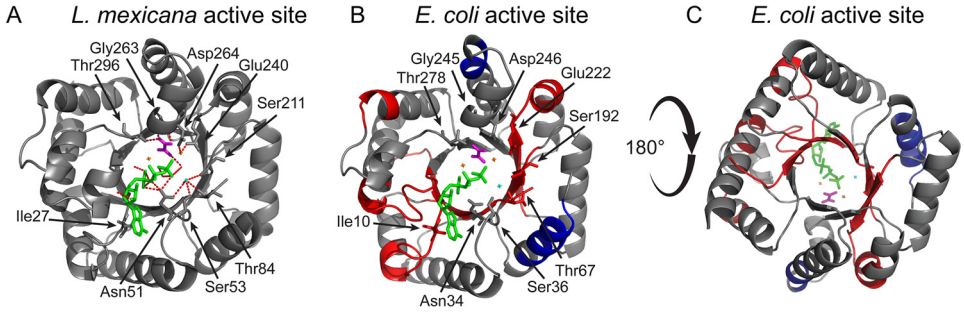

FIGURE 9. **Dynamic changes to the catalytic site of the $(\beta/\alpha)_8$-barrel.** *A*, *L. mexicana* $(\beta/\alpha)_8$-barrel showing how the substrates bound in the active site (Protein Data Bank code 3HQP). Hydrogen bonds between the substrates and residues are shown in *red* with interacting residues shown as *sticks* and labeled. The substrates bound in the active site are colored as follows: ATP, *green*; pyruvate, *magenta*; magnesium ions, *orange*; and potassium ion, *cyan*. *B*, *E. coli* type 1 pyruvate kinase $(\beta/\alpha)_8$-barrel (looking down the barrel). The active site substrates and equivalent interacting residues are modeled from the *L. mexicana* crystal structure (Protein Data Bank code 3HQP) and presented as *sticks* and labeled. *C*, *E. coli* type 1 pyruvate kinase $(\beta/\alpha)_8$-barrel (looking up the barrel).

Overall, the peptides mapped to the tetrameric interfaces demonstrate increased conformational flexibility, indicating that the interfaces are destabilized upon fructose 1,6-bisphosphate binding. Interestingly, this result, together with the increased conformational sampling evidenced from the global hydrogen-deuterium exchange experiment above, contradicts the general hypothesis put forward by Morgan *et al.* (10) that "while the regulatory molecules and molecular mechanisms may vary between species, the underlying principle of tetrameric stabilization in response to effector binding is conserved." That study used thermal unfolding to infer conformation stability, whereas the data from the hydrogen-deuterium exchange directly assess the degree of conformational flexibility both globally and within specific regions within the protein. In any event, together with the dramatic destabilization at the A/C interdomain interface Cα4′-helix (peptide 398–408), our results connect the domain and tetrameric interfaces and in particular their destabilization to the allosteric mechanism of *E. coli* pyruvate kinase type 1 enzyme (30).

Lastly, our data are consistent with the effect that fructose 1,6-bisphosphate has on phosphoenolpyruvate affinity. Fructose 1,6-bisphosphate binding blocks the homotropic allosteric mechanism by phosphoenolpyruvate: in the absence of fructose 1,6-bisphosphate, titration of phosphoenolpyruvate results in a sigmoidal response, a signature of cooperativity, whereas in the presence of fructose 1,6-bisphosphate a rectangular hyperbolic curve is observed, signaling a loss of cooperativity. Destabilization of the domain and tetrameric interfaces, such that the active site-containing A-domains are decoupled from one another, is consistent with the loss of phosphoenolpyruvate cooperation between active sites.

Signaling the Catalytic Site for Activation—Next, we traced changes in conformational flexibility associated with the active site $(\beta/\alpha)_8$-barrel domain to understand the mechanism by which fructose 1,6-bisphosphate binding affects catalysis.

Increased conformational flexibility of the β-strands within the $(\beta/\alpha)_8$-barrel accompanies destabilization of the Cα4′-helix, which sits at the interdomain interface between the allosteric and catalytic domains and interacts with the $\alpha\beta$-loops at the N terminus of the $(\beta/\alpha)_8$-barrel. Residue Gln^{408} of the key Cα4′-helix forms interactions with Asp^{187} of loop $\alpha_3\beta_3$ and Asn^{214} of loop $\alpha_4\beta_4$, whereas Lys^{404} of the Cα4′-helix interacts with Gly^{185} of loop $\alpha_3\beta_3$ (Fig. 7*E*). Given the large change in conformational flexibility of the Cα4′-helix, unsurprisingly, the β-strands following the $\alpha\beta$-loops (β-strands 4 and 5, respectively) show an increase in deuterium exchange of 23 and 31%, respectively. Furthermore, β-strands 1, 2, and 3 also showed some destabilization (increase in deuterium exchange of 36, 22, and 27%, respectively), resulting in a largely unstable $(\beta/\alpha)_8$-barrel core. The destabilization of these β-strands suggests that the allosteric signal is communicated through the core of the $(\beta/\alpha)_8$-barrel to the active site.

Changes in deuterium exchange were also identified in the active site loops at the top of the $(\beta/\alpha)_8$-barrel (Fig. 9). Exchange in the peptide containing the $\beta_8\alpha_8$ loop increased by 20%, and the peptide containing the neighboring $\beta_1\alpha_1$ increased by 36%. Furthermore, β-strands 1, 2, 3, 4, and 5 in the core of the $(\beta/\alpha)_8$-barrel near the substrate binding sites were also destabilized. Specific substrate binding regions are modeled from *L. mexicana* pyruvate kinase crystal structures (Protein Data Bank code 3HQP). This reveals that the adenosine ring of the ATP (or ADP) is located within interaction distance of loops $\beta_1\alpha_1$, $\beta_2\alpha_2$, $\beta_3\alpha_3$, and $\beta_8\alpha_8$, whereas the oxalate molecule (an analogue of phosphoenolpyruvate/pyruvate) and catalytic ions are situated near β-strands 4 and 5 (Fig. 9). Thus, many of the catalytically important residues show increased conformational flexibility. A caveat to this analysis is that the peptides, in addition to residues belonging to β-strands 1, 3, and 4, also include residues that are with the $\beta\alpha$-loops, which are likely to be dynamic. Unfortunately, the resolution limits of this experiment do not allow us to confirm whether the loop regions are experiencing high exchange, thus causing an averaged apparent high exchange of the peptide, or whether the entire peptide is experiencing high exchange.

Increased exchange in these specific active site loops in the *E. coli* pyruvate kinase type 1 enzyme implies that substrate binding is likely conserved across pyruvate kinase enzymes and that the binding of fructose 1,6-bisphosphate increases the flexibility of these active site loops (Fig. 9). Structural analysis comparing temperature factors of the *L. mexicana* structures in the presence and absence of fructose 1,6-bisphosphate identifies two active site loops ($\beta_7\alpha_7$ and $\beta_8\alpha_8$) and their preceding β-strands (7 and 8) in the core of the $(\beta/\alpha)_8$-barrel that have increased B-factors upon fructose 1,6-bisphosphate binding. Increased B-factors in these active site regions suggest that allosteric activation by fructose 1,6-bisphosphate binding

increases the flexibility of active site loops for substrate and catalytic ion binding. The binding of the allosteric activator can redistribute protein conformational ensembles and alter the rates of interchange between these populations; this can manifest as a change in flexibility at the active site (27). The increased exchange can be explained by these loops having greater flexibility and therefore an increased range of conformational sampling, which would increase the chances of substrate binding for catalysis (50, 51). Increased exchange in the active site at early labeling time points is consistent with the "intensification" model for catalysis-linked dynamics whereby the energy barrier between conformational substates is lowered upon activator binding (46). This supports the K-type binding mechanism, which proposes that allosteric activation increases the binding affinity of substrate in the active site (5).

The Flexible Lid Domain (B-domain) Is Not Allosterically Controlled by Fructose 1,6-Bisphosphate—The exchange profiles of peptides derived from the lid domain (B-domain) of pyruvate kinase type 1 are largely unchanged when the enzyme is pretreated with fructose 1,6-bisphosphate, suggesting that ligand binding in the allosteric site has only a minor effect upon the secondary structure of the lid domain. This result is consistent with previous studies that have shown that the movement of the flexible lid domain is not allosterically controlled (17, 21, 52); however, it is controlled by the presence, type, and position of substrates bound within the active site.

Conclusion—The results presented here provide an experimental characterization of site-specific dynamics for the allosteric activation of *E. coli* pyruvate kinase type 1, a central metabolic enzyme. The deuterium exchange data demonstrate that fructose 1,6-bisphosphate binding alters the conformational flexibility of specific regions, largely increasing the conformational sampling in the bound state. In addition, the data reveal altered dynamics in the allosteric binding region and also at the substrate binding site ~40 Å away. The results are consistent with the view of allosteric activation that describes proteins as dynamic molecules existing as an ensemble of conformations (40, 41, 44), fluctuating between conformational states toward which the favored states can be shifted by the allosteric event (24, 25, 27, 43, 44).

Based on our interpretation of the observed dynamic changes during the allosteric transition to the active bound state, we propose that the following scheme results in allosteric activation of *E. coli* pyruvate kinase type 1 upon fructose 1,6-bisphosphate binding 1) The presence of fructose 1,6-bisphosphate destabilizes the effector loop and causes a structural rearrangement, displacing it to allow binding. 2) The fructose 1,6-bisphosphate then forms interactions with the Cα3′-helix, increasing the stability of the helix and weakening an interaction between the loop preceding Cα3′ and the Cα4′-helix. 3) Destabilization of the Cα4′-helix results in destabilization of the interdomain interface that links the allosteric domain (C-domain) and the $(\beta/\alpha)_8$-barrel (A-domain) within the monomer. 4) Altered interactions of the destabilized Cα4′-helix at the interface between the A- and C-domains and loops $\alpha_3\beta_3$ and $\alpha_4\beta_4$ result in destabilized β-strands following the $\alpha\beta$-loops, consequently producing a more conformationally flexible $(\beta/\alpha)_8$-barrel core. This destabilization is consistent with the β-strands being involved in allosteric signal transfer through the core of the $(\beta/\alpha)_8$-barrel to the active site. 5) The signal transfer through the core of the $(\beta/\alpha)_8$-barrel destabilizes the substrate binding loops at the active site. We propose that the active site loops then sample a greater number of conformations, some of which facilitate binding of the substrate and catalytic ions. 6) The destabilization of the tetrameric interfaces (A/A′ and C/C′) decouples the monomers attenuating the phosphoenolpyruvate homotropic allosteric signal between active sites, explaining why fructose 1,6-bisphosphate binding blocks the phosphoenolpyruvate allosteric mechanism.

In conclusion, we propose a new mechanism by which fructose 1,6-bisphosphate allosterically regulates pyruvate kinase. This work extends previous knowledge of the allosteric activation mechanism by explaining how fructose 1,6-bisphosphate promotes substrate binding and attenuating the phosphoenolpyruvate homotropic allosteric signal despite the allosteric binding site being 40 Å away from the active site.

Author Contributions—K. A. D., R. C. J. D., and D. J. W. designed and coordinated the study and wrote the article with the help of S. A. K. K. A. D., S. Z., F. P., and P. L. designed, performed, and analyzed the experiments. All authors were involved in the interpretation of the data. All authors critically revised the article, reviewed the results, and approved the final version of the manuscript.

Acknowledgments—We thank Grant Pearce and Jeremy Keown for graphic assistance. We acknowledge Jackie Healy for effervescent technical support.

References

1. Fenton, A. W. (2008) Allostery: an illustrated definition for the second secret of life. *Trends Biochem. Sci.* **33,** 420–425
2. Changeux, J. P. (2013) 50 years of allosteric interactions: the twists and turns of the models. *Nat. Rev. Mol. Cell Biol.* **14,** 819–829
3. Monod, J., Changeux, J. P., and Jacob, F. (1963) Allosteric proteins and cellular control systems. *J. Mol. Biol.* **6,** 306–329
4. Yuan, Y., Tam, M. F., Simplaceanu, V., and Ho, C. (2015) New look at hemoglobin allostery. *Chem. Rev.* **115,** 1702–1724
5. del Sol, A., Tsai, C. J., Ma, B., and Nussinov, R. (2009) The origin of allosteric functional modulation: multiple pre-existing pathways. *Structure* **17,** 1042–1050
6. Ponce, E., Flores, N., Martinez, A., Valle, F., and Bolívar, F. (1995) Cloning of the two pyruvate kinase isoenzyme structural genes from *Escherichia coli*: the relative roles of these enzymes in pyruvate biosynthesis. *J. Bacteriol.* **177,** 5719–5722
7. Muirhead, H., Clayden, D. A., Barford, D., Lorimer, C. G., Fothergill-Gilmore, L. A., Schiltz, E., and Schmitt, W. (1986) The structure of cat muscle pyruvate kinase. *EMBO J.* **5,** 475–481
8. Mattevi, A., Valentini, G., Rizzi, M., Speranza, M. L., Bolognesi, M., and Coda, A. (1995) Crystal structure of *Escherichia coli* pyruvate kinase type I: molecular basis of the allosteric transition. *Structure* **3,** 729–741
9. Jeoung, N. H., Harris, C. R., and Harris, R. A. (2014) Regulation of pyruvate metabolism in metabolic-related diseases. *Rev. Endocr. Metab. Disord.* **15,** 99–110
10. Morgan, H. P., Zhong, W., McNae, I. W., Michels, P. A., Fothergill-Gilmore, L. A., and Walkinshaw, M. D. (2014) Structures of pyruvate kinases display evolutionarily divergent allosteric strategies. *R. Soc. Open. Sci.* **1,** 140120
11. Jurica, M. S., Mesecar, A., Heath, P. J., Shi, W., Nowak, T., and Stoddard, B. L. (1998) The allosteric regulation of pyruvate kinase by fructose-1,6-bisphosphate. *Structure* **6,** 195–210

12. Monod, J., Wyman, J., and Changeux, J. P. (1965) On the nature of allosteric transitions: a plausible model. *J. Mol. Biol.* **12,** 88–118
13. Muñoz, M. E., and Ponce, E. (2003) Pyruvate kinase: current status of regulatory and functional properties. *Comp. Biochem. Physiol. B Biochem. Mol. Biol.* **135,** 197–218
14. Waygood, E. B., Rayman, M. K., and Sanwal, B. (1975) The control of pyruvate kinases of *Escherichia coli.* II. Effectors and regulatory properties of the enzyme activated by ribose 5-phosphate. *Can. J. Biochem.* **53,** 444–454
15. Fothergill-Gilmore, L. A., and Michels, P. A. (1993) Evolution of glycolysis. *Prog. Biophys. Mol. Biol.* **59,** 105–235
16. Allen, S. C., and Muirhead, H. (1996) Refined three-dimensional structure of cat-muscle (M1) pyruvate kinase at a resolution of 2.6 Å. *Acta Crystallogr. D Biol. Crystallogr.* **52,** 499–504
17. Morgan, H. P., McNae, I. W., Nowicki, M. W., Hannaert, V., Michels, P. A., Fothergill-Gilmore, L. A., and Walkinshaw, M. D. (2010) Allosteric mechanism of pyruvate kinase from *Leishmania mexicana* uses a rock and lock model. *J. Biol. Chem.* **285,** 12892–12898
18. Levine, M., Muirhead, H., Stammers, D. K., and Stuart, D. I. (1978) Structure of pyruvate kinase and similarities with other enzymes: possible implications for protein taxonomy and evolution. *Nature* **271,** 626–630
19. Kumar, S., and Barth, A. (2011) Effects of ions on ligand binding to pyruvate kinase: mapping the binding site with infrared spectroscopy. *J. Phys. Chem. B* **115,** 6784–6789
20. Ishwar, A., Tang, Q., and Fenton, A. W. (2015) Distinguishing the interactions in the fructose-1,6-bisphosphate binding site of human liver pyruvate kinase that contribute to allostery. *Biochemistry* **54,** 1516–1524
21. Zhong, W., Morgan, H. P., Nowicki, M. W., McNae, I. W., Yuan, M., Bella, J., Michels, P. A., Fothergill-Gilmore, L. A., and Walkinshaw, M. D. (2014) Pyruvate kinases have an intrinsic and conserved decarboxylase activity. *Biochem. J.* **458,** 301–311
22. Mattevi, A., Bolognesi, M., and Valentini, G. (1996) The allosteric regulation of pyruvate kinase. *FEBS Lett.* **389,** 15–19
23. Mattevi, A., Rizzi, M., and Bolognesi, M. (1996) New structures of allosteric proteins revealing remarkable conformational changes. *Curr. Opin. Struct. Biol.* **6,** 824–829
24. Tsai, C. J., and Nussinov, R. (2014) A unified view of "how allostery works." *PLoS Comput. Biol.* **10,** e1003394
25. Boehr, D. D., Nussinov, R., and Wright, P. E. (2009) The role of dynamic conformational ensembles in biomolecular recognition. *Nat. Chem. Biol.* **5,** 789–796
26. Motlagh, H. N., Wrabl, J. O., Li, J., and Hilser, V. J. (2014) The ensemble nature of allostery. *Nature* **508,** 331–339
27. Goodey, N. M., and Benkovic, S. J. (2008) Allosteric regulation and catalysis emerge via a common route. *Nat. Chem. Biol.* **4,** 474–482
28. Suzuki, H., Tabata, K., Morita, E., Kawasaki, M., Kato, R., Dobson, R. C., Yoshimori, T., and Wakatsuki, S. (2014) Structural basis of the autophagy-related LC3/Atg13 LIR complex: recognition and interaction mechanism. *Structure* **22,** 47–58
29. Malcovati, M., and Valentini, G. (1982) AMP- and fructose 1,6-bisphosphate-activated pyruvate kinases from *Escherichia coli*. *Methods Enzymol.* **90,** 170–179
30. Valentini, G., Chiarelli, L., Fortin, R., Speranza, M. L., Galizzi, A., and Mattevi, A. (2000) The allosteric regulation of pyruvate kinase: a site-directed mutagenesis study. *J. Biol. Chem.* **275,** 18145–18152
31. Hill, A. (1910) The possible effects of the aggregation of the molecules of haemoglobin on its dissociation curves. *J. Phys.* **40,** i–vii
32. Rob, T., Liuni, P., Gill, P. K., Zhu, S., Balachandran, N., Berti, P. J., and Wilson, D. J. (2012) Measuring dynamics in weakly structured regions of proteins using microfluidics-enabled subsecond H/D exchange mass spectrometry. *Anal. Chem.* **84,** 3771–3779
33. Rob, T., and Wilson, D. J. (2009) A versatile microfluidic chip for millisecond time-scale kinetic studies by electrospray mass spectrometry. *J. Am. Soc. Mass Spectrom.* **20,** 124–130
34. Wilson, D. J., and Konermann, L. (2003) A capillary mixer with adjustable reaction chamber volume for millisecond time-resolved studies by electrospray mass spectrometry. *Anal. Chem.* **75,** 6408–6414
35. Zhu, T., Bailey, M. F., Angley, L. M., Cooper, T. F., and Dobson, R. C. (2010) The quaternary structure of pyruvate kinase type 1 from *Escherichia coli* at low nanomolar concentrations. *Biochimie* **92,** 116–120
36. Fenton, A. W., and Blair, J. B. (2002) Kinetic and allosteric consequences of mutations in the subunit and domain interfaces and the allosteric site of yeast pyruvate kinase. *Arch. Biochem. Biophys.* **397,** 28–39
37. Boiteux, A., Markus, M., Plesser, T., Hess, B., and Malcovati, M. (1983) Analysis of progress curves. Interaction of pyruvate kinase from *Escherichia coli* with fructose 1,6-bisphosphate and calcium ions. *Biochem. J.* **211,** 631–640
38. Resetca, D., Haftchenary, S., Gunning, P. T., and Wilson, D. J. (2014) Changes in signal transducer and activator of transcription 3 (STAT3) dynamics induced by complexation with pharmacological inhibitors of Src homology 2 (SH2) domain dimerization. *J. Biol. Chem.* **289,** 32538–32547
39. Strohalm, M., Kavan, D., Novák, P., Volný, M., and Havlícek, V. (2010) mMass 3: a cross-platform software environment for precise analysis of mass spectrometric data. *Anal. Chem.* **82,** 4648–4651
40. Kerns, S. J., Agafonov, R. V., Cho, Y. J., Pontiggia, F., Otten, R., Pachov, D. V., Kutter, S., Phung, L. A., Murphy, P. N., Thai, V., Alber, T., Hagan, M. F., and Kern, D. (2015) The energy landscape of adenylate kinase during catalysis. *Nat. Struct. Mol. Biol.* **22,** 124–131
41. Frauenfelder, H., Sligar, S. G., and Wolynes, P. G. (1991) The energy landscapes and motions of proteins. *Science* **254,** 1598–1603
42. Ma, B., Tsai, C. J., Haliloğlu, T., and Nussinov, R. (2011) Dynamic allostery: linkers are not merely flexible. *Structure* **19,** 907–917
43. Nussinov, R., and Tsai, C. J. (2015) Allostery without a conformational change? Revisiting the paradigm. *Curr. Opin. Struct. Biol.* **30,** 17–24
44. Smock, R. G., and Gierasch, L. M. (2009) Sending signals dynamically. *Science* **324,** 198–203
45. Boehr, D. D., McElheny, D., Dyson, H. J., and Wright, P. E. (2006) The dynamic energy landscape of dihydrofolate reductase catalysis. *Science* **313,** 1638–1642
46. Liuni, P., Jeganathan, A., and Wilson, D. J. (2012) Conformer selection and intensified dynamics during catalytic turnover in chymotrypsin. *Angew. Chem. Int. Ed. Engl.* **51,** 9666–9669
47. Morgan, H. P., McNae, I. W., Nowicki, M. W., Zhong, W., Michels, P. A., Auld, D. S., Fothergill-Gilmore, L. A., and Walkinshaw, M. D. (2011) The trypanocidal drug suramin and other trypan blue mimetics are inhibitors of pyruvate kinases and bind to the adenosine site. *J. Biol. Chem.* **286,** 31232–31240
48. Walker, D., Chia, W. N., and Muirhead, H. (1992) Key residues in the allosteric transition of *Bacillus stearothermophilus* pyruvate kinase identified by site-directed mutagenesis. *J. Mol. Biol.* **228,** 265–276
49. Lovell, S. C., Mullick, A. H., and Muirhead, H. (1998) Cooperativity in *Bacillus stearothermophilus* pyruvate kinase. *J. Mol. Biol.* **276,** 839–851
50. Urfer, R., and Kirschner, K. (1992) The importance of surface loops for stabilizing an eightfold $\beta\alpha$ barrel protein. *Protein Sci.* **1,** 31–45
51. Eisenmesser, E. Z., Millet, O., Labeikovsky, W., Korzhnev, D. M., Wolf-Watz, M., Bosco, D. A., Skalicky, J. J., Kay, L. E., and Kern, D. (2005) Intrinsic dynamics of an enzyme underlies catalysis. *Nature* **438,** 117–121
52. Fenton, A. W., Williams, R., and Trewhella, J. (2010) Changes in small angle x-ray scattering parameters observed upon ligand binding to rabbit muscle pyruvate kinase are not correlated with allosteric transitions. *Biochemistry* **49,** 7202–7209
53. Donovan, K. A., Atkinson, S. A., Kessans, S. A., Peng, F., Cooper, T. F., Griffin, M. D. W., Jameson, G. B., and Dobson, R. C. (2016) Grappling with anisotropic data, pseudo-merohedral twinning and pseudo-translational non-crystallographic symmetry: a case study involving pyruvate kinase. *Acta Crystallogr. D Biol. Crystallogr.* 10.1107/S205979831600142X